DOI: 10.1002/adma.200601191

Rapid Fabrication of Uniformly Sized Nanopores and Nanopore Arrays for Parallel DNA Analysis**

By *Min Jun Kim*, *Meni Wanunu*, *David C. Bell*, and *Amit Meller**

Nanometer-sized pores can be used to detect and characterize biopolymers, such as DNA, RNA, and polypeptides, with single-molecule resolution. Experiments performed with the 1.5 nm pore α-hemolysin (α-HL)[1] demonstrated that single-stranded DNA and RNA molecules can be electrophoretically threaded through a pore, and that the ion current flowing through the pore contains information about the biopolymer sequence: its type, length, and secondary structure.[2,3] The α-HL nanopore has been used to study the unzipping kinetics of DNA hairpin molecules under stationary or time-varying forces,[4] to detect DNA hybridization kinetics,[5] and to study the interaction of DNA with bound proteins using nanopore force spectroscopy.[6] In addition, α-HL can be biochemically modified for various sensing tasks, such as analyte detection and ligand–receptor interactions.[7]

Solid-state nanopores can be fabricated in thin Si_3N_4 and SiO_2 membranes, using either an Ar^+ beam[8,9] or an electron beam (e-beam) in a transmission electron microscope (TEM),[10] as well as in a variety of materials using other techniques.[11] Solid-state nanopores offer several advantages over phospholipid-embedded protein channels, namely, their size can be tuned with nanometer precision and they exhibit an increased mechanical, chemical, and electrical stability. Recent studies using solid-state pores have begun to emerge, demonstrating the detection of single-stranded and double-stranded DNA molecules.[12,13] A major advantage of solid-state nanopores is that they can, in principle, be integrated into devices compatible with other detection schemes in addition to ion current measurements. In particular, optical-based methods offer straightforward parallelism through the simultaneous probing of many nanopores. Optical methods for sensing single molecules can be implemented by labeling the biomolecules and/or the nanopores. Although protein pores embedded in a phospholipid bilayer can be interrogated optically to detect single molecules,[14] a stable, long-timescale probing is very complicated since the pores readily diffuse in the bilayer, leading to aggregation and destabilization of the membrane. In contrast, nanopores fabricated in solid-state materials are static, and are therefore more compatible with optical probing.

In this paper, we extend state-of-the-art techniques by demonstrating the rapid fabrication of finely tuned nanopores and nanopore arrays. The nanopores were fabricated in thin Si_3N_4 films using the intense e-beam of a field-emission TEM. By maximizing the e-beam density at the specimen we achieved a nearly fivefold decrease in the fabrication time of a single nanopore (ca. 30 s).[15,16] Investigation of pore contraction/expansion dynamics[17] under different irradiation conditions enabled nanopore fabrication in the range of 2–20 nm with exceptional size control (<0.5 nm variability). Since the nanopores were fabricated sequentially (i.e., using one e-beam), both the reduction in fabrication time and size control were crucial for the manufacturing of nanopore arrays. The 3D nanopore shape was extensively characterized by performing TEM tomography, as well as by ion-current measurements through the pores. Finally, the detection of double-stranded DNA molecules through 4 nm diameter nanopores was demonstrated by monitoring their translocation under an applied bias.

The starting materials for TEM processing were either fabricated in house or by Protochips Inc. (Raleigh, NC), using the following procedure: low-pressure chemical vapor deposition (LPCVD) was used to form a Si_3N_4 film (20 or 50 nm thick) on one side of a 500 μm thick Si wafer. A 100 μm × 100 μm window was then fabricated in the wafer using photolithography and standard wet-etching. Nanopore fabrication was then carried out in the thin Si_3N_4 membrane using a JEOL 2010F field-emission TEM. Alignment of the e-beam involved the adjustment of the condenser stigmatism to the familiar triangle-shaped beam,[18] using a large condenser aperture. The resulting electron-energy-density distribution displayed a threefold aberration. The condenser lens was then used to fully converge the beam to an intense point with a triangular halo of low intensity. The column was then aligned using standard high-resolution transmission electron microscopy alignment procedures. After the alignment procedure, nanopores with diameters (d) in a range from 3 to 6 nm were directly drilled using an e-beam intensity of ca. 2.5×10^8 e nm^{-2} and a

[*] Dr. A. Meller, Dr. M. J. Kim, Dr. M. Wanunu
Department of Biomedical Engineering
and Department of Physics
Boston University, Boston, MA 02215 (USA)
E-mail: ameller@bu.edu
D. C. Bell
Division of Engineering & Applied Science and
The Center for Nanoscale Systems
Harvard University, Cambridge, MA 02138 (USA)

[**] Meni Wanunu and Min Jun Kim both contributed equally to this work. This work was supported by the National Science Foundation grant NIRT 0403891, and the National Institute of Health grant HG 003574. The authors thank staff from the Center for Nanoscale Systems (CNS) and the Rowland Institute at Harvard for technical assistance. We acknowledge stimulating conversations with Dr. S. Lemay and Dr. D. Krapf in the initial phase of the research, and Dr. K. Murata for his assistance in TEM tomography.

ADVANCED MATERIALS

magnification of 800 000×.[19] The time for pore formation in a 50 nm thick Si_3N_4 membrane was ca. 30 s for a 200 keV beam. Manipulation of the e-beam intensity resulted in controlled contraction/expansion, which was used to fabricate the desired nanopore diameter.[10]

Our nanopore-drilling procedure consisted of three main stages, as shown in Figure 1: I) nanopore formation, II) controlled expansion or contraction, and III) controlled expansion. Note that during stage II, both expansion and contraction could be achieved by manipulating the electron beam.

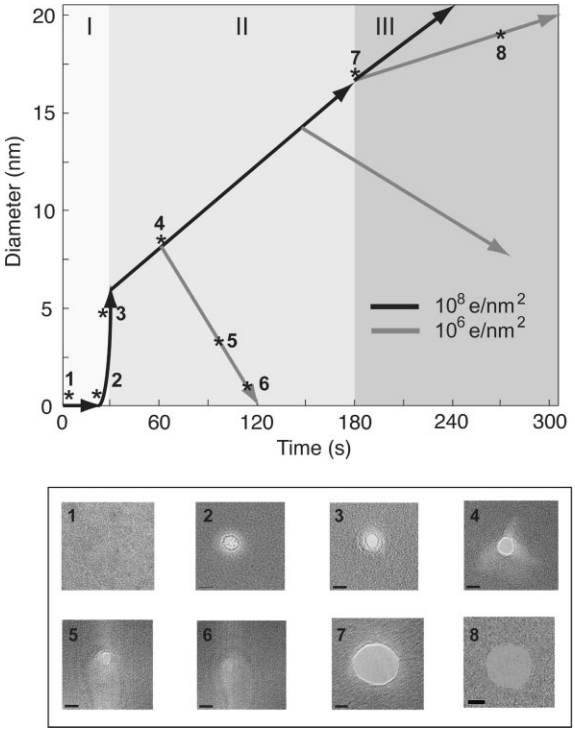

Figure 1. Top panel: steps during the fabrication of solid-state nanopores in a Si_3N_4 membrane using a TEM. The diagram displays the average nanopore diameter as a function of the irradiation time. Three stages are identified: I) initial pore formation and rapid growth; II) controlled expansion or contraction (e-beam intensity dependent); and III) controlled expansion. High e-beam intensity is shown by the black arrows (10^8 e nm^{-2}); low e-beam intensity is shown by the gray arrows (10^6 e nm^{-2}). Bottom panels: transmission electron microscopy images of the nanopores at various steps. Insets 1 and 2 display the Si_3N_4 membrane before pore formation. The scale bars correspond to 5 nm where displayed.

Insets display transmission electron microscopy images of the Si_3N_4 membrane at various stages: 1–3 during stage I; 4–6 during the contraction in stage II; and 7–8 during the expansion in stage III. The black and gray arrows correspond to either high or low e-beam intensity, respectively. The process could be terminated after each of these steps, when the desired size had been attained.

Nanopore contraction has previously been observed for nanopores fabricated in SiO_2 membranes, attributed to the e-beam induced fluidization of the nanopore walls.[10] In our study, a similar phenomenon was observed with Si_3N_4 membranes, which are mechanically superior.[16,20] We investigated the dynamics of contraction or expansion under constant irradiation (10^6 e nm^{-2}) by comparing nanopores with different initial nanopore sizes (d_0). Our results are shown in Figure 2. The contraction/expansion dynamics were found to be roughly linear in time and were characterized by the rate, $r(d_0)$. The rate vanishes at a critical initial pore size $d_c \approx 16$ nm, as shown in the inset. For $d_0 > d_c$, the pores expand with a rate that grows with d_0, but for $d_0 < d_c$ the pores contract (negative r) with a rate that grows for smaller initial pores. These results were highly reproducible: repeating the experiment five times with different pores (with the same d_0 and beam intensity) yielded similar dynamics. The scatter of the results is reflected in the error bars.

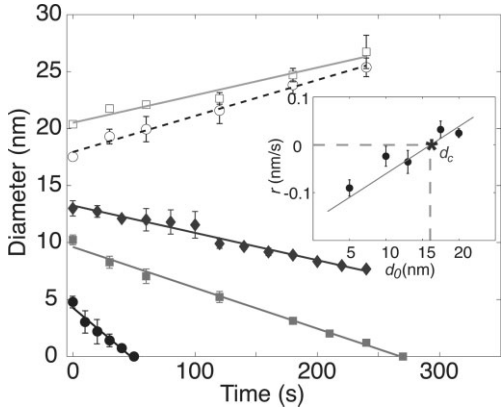

Figure 2. Nanopore expansion or contraction dynamics for a fixed e-beam intensity of 10^6 e nm^{-2}, as a function of the initial nanopore diameter, d_0. The different symbols represent different d_0 values at $t = 0$. The average diameter as a function of time is displayed. A uniform contraction or expansion is observed for nanopores with d_0 below and above the critical size $d_c = 16$ nm, respectively. The inset depicts the rate of contraction or expansion as a function of d_0.

Storm et al. have shown that if nanopore contraction is driven entirely by surface-energy minimization of a perfect cylinder, then $d_c = h$, where h is the membrane thickness.[10] Our results indicate that $d_c \approx 1/3\,h$ (Fig. 2). To explain this apparent discrepancy and to further explore the pore geometry we used TEM tomography[21] in order to obtain a reconstructed 3D image of the nanopore. Our results (Fig. 3) clearly suggest a truncated double-cone pore structure, with a uniform constriction in the center of the membrane. The conical structure effectively reduces the membrane thickness of the nanopore by roughly a factor of three, such that $h_{eff} \approx 1/3\,h$ (Fig. 3 inset). This results in $h_{eff} \approx d_c$, which is in agreement with results reported by Storm et al. We cannot rule out, however, that the more realistic cone-shape geometry leads to a different dependence of d_c on h that cannot be predicted from the simple cylindrical approximation, or that the specific material properties played a role (Storm et al. used SiO_2).

The rapid fabrication of uniform nanopores with known shape implies that nanopore arrays can provide a viable

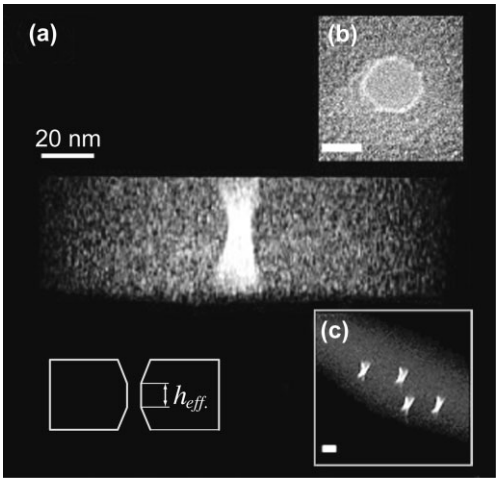

Figure 3. a) A reconstructed side view obtained by TEM tomography of a 7 nm nanopore in a 50 nm thick Si_3N_4 membrane, revealing a truncated double-cone structure (shown schematically below the image). b) A high-resolution top-view image of the same pore (scale bar is 5 nm). c) A tilted view of a 2×2 nanopore array (7 nm diameters) imaged using TEM tomography. The spacing between pores in the array is 50 nm (scale bar is 10 nm).

means for parallel analysis of single DNA molecules. Due to the enormous number of applications that could potentially use parallel analysis, spatially patterned nanopore arrays have gained attention in recent years.[9,22] Towards this end, we developed two approaches for nanopore-array fabrication. The first approach involved a preliminary definition of a well array, used as nanometer-sized landmarks for subsequent nanopore fabrication. These wells are fabricated by focused ion beam (FIB) etching of the first Si_3N_4 layer in a three-layer structure ($Si_3N_4/SiO_2/Si_3N_4$), as shown in Figure 4a, followed by wet-etching of the SiO_2 layer by buffered oxide etch (BOE). Nanopore drilling was then carried out inside the wells as explained above. A further advantage of the well structure is that it facilitates optical probing of the nanopores, as the wells mark the approximate positions of the nanopores. Figure 4b shows a 6×6 array of defined wells in which nanopores have been fabricated using a TEM. Figure 4d displays the size distribution of the 36 nanopores in this array, fitted by normal distribution (gray line). The average size of these nanopores is 5.14 nm with a standard deviation of 0.46 nm.

The second approach involves drilling in a Si_3N_4 membrane using automated scanning transmission electron microscopy (STEM), which enables custom-patterning of the nanopore array. This is achieved by directly addressing the scan coils to deflect the beam by a desired amount, producing the array in a rapid, flexible, and automated fashion. An example of a 2×2 square array of 20 nm pores fabricated using STEM is shown in Figure 4c. The size of the nanopores shown was chosen for visualization, as smaller pores would not be discernable at this magnification. The fabrication time for the array shown in Figure 4c was less than 10 min, a significant reduction in time compared with the first approach (ca. 12 h). The average size of the four pores is (20.1 ± 0.2) nm. As shown in

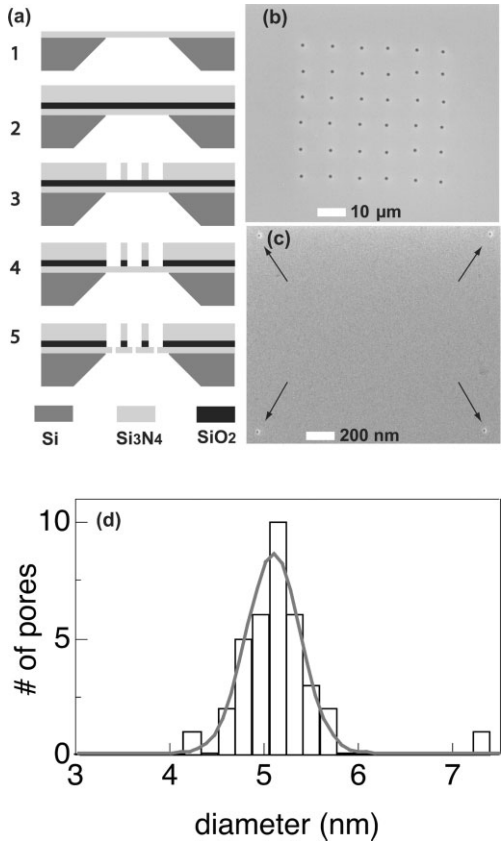

Figure 4. a) A schematic illustration of the fabrication steps involved in nanopore array preparation: 1) definition of a 50 nm Si_3N_4 membrane window; 2) deposition of 200 nm thick SiO_2 and 500 nm thick Si_3N_4 layers using plasma-enhanced chemical vapor deposition (PECVD); 3) fabrication of a 2 µm diameter well array using a FIB in the Si_3N_4 layer; 4) removal of the SiO_2 layer; and 5) nanopore drilling in each well using a TEM, as in Figure 1. b) A TEM image of a 6×6 array of 2 µm wells, each well containing a 5 nm pore. c) A 2×2 nanopore array fabricated by automated scanning transmission electron microscopy (STEM) in a 50 nm Si_3N_4 membrane window (2 µm distances between 20 nm diameter nanopores). d) The size distribution of 36 nanopores fabricated in the 6×6 well array in (b).

Figure 3c, smaller array spacing and diameters can be readily achieved with this method. Finally, the size distribution of the STEM-generated pores was checked by producing a 3×3 array of 10 nm nanopores similar to Figure 3c. Analysis of the sizes reveals an average size of (9.3×0.6) nm, indicating that the automated process can be used with no compromise in accuracy.

We have characterized the ionic conductivity of our nanopores by performing a set of current–voltage (I–V) measurements at different ionic strengths. In all cases, from 3 to 15 nm, the nanopores exhibit Ohmic behavior in the range –0.5 to +0.5 V. The slope of the I–V curves was used to determine the pore conductivity, G. Based on the TEM-tomography information (Fig. 3), we derive an equation for the ionic conductivity through a truncated double-cone structure (neglecting surface-induced flow due to the shielding counterions)[23]

ADVANCED MATERIALS

$$G = \frac{\pi d^2}{4}\sigma\left(\frac{\delta \tan\alpha + 1}{h + h_{\text{eff}}\delta \tan\alpha}\right) \quad (1)$$

where $\sigma = (\mu_K + \mu_{Cl})\eta_{KCl}e$ is the specific conductance at a number density η_{KCl}, equal to 15.04 and 3.01 $\Omega^{-1}\,m^{-1}$ for 1 and 0.2 M KCl, respectively (η_K and η_{Cl} are the electrophoretic mobilities of K^+ and Cl^-, respectively, and e is the elementary charge unit ($e = -1.602 \times 10^{-19}$ C)); $\delta = (h - h_{\text{eff}})/d$; h_{eff} is the width of the cylindrical region in the nanopore; and α is the cone half-angle. The dependence of G on the pore diameter is shown in Figure 5. The inset depicts our idealized model for the nanopore structure. Using known values for σ and $h = 50$ nm we fit our data with Equation 1 using two free variables (h_{eff} and α). From these fits (solid lines) we obtain $h_{\text{eff}} = (17 \pm 1)$ and (18 ± 1) nm for the 1 and 0.2 M data, respectively, and $\alpha = 30° \pm 2°$ for both cases. These results are in a good agreement with the 3D reconstructed image obtained by TEM tomography (Fig. 3). In particular, we note that $h_{\text{eff}}/h \approx 2.9$, which is close to our estimate from the TEM image. Conductivity measurements of a 3×3 nanopore array with $d = (9.3 \pm 0.8)$ nm yield 360 nS, which is in agreement with the expected conductivity of nine pores of the same diameter (330 nS).

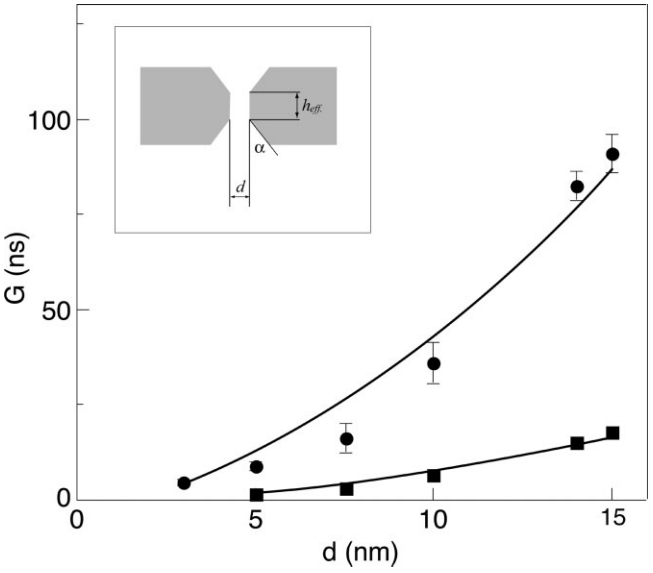

Figure 5. Ionic conductance (G) of solid-state nanopores as a function of their diameter measured in 1.0 (circles) and 0.2 M (squares) KCl solution. The lines represent fits to Equation 1 assuming a truncated double-cone structure, as shown in the inset.

To demonstrate the functionality of the nanopores we performed DNA translocation experiments, similar to those reported for α-HL[3] and solid-state pores.[8,10,13] Each nanopore chip was mounted onto a custom-built cell that contained two miniature fluid chambers. The chambers were fitted with ports for Ag/AgCl electrodes connected to an Axopatch 200B headstage. Signals were low-pass filtered at 20 kHz using a Butterworth filter and digitized at 100 kHz (12 bit). Figure 6 displays ion-current blockades produced by applying 10 nM of 150 bp (bp = base pair) double-stranded DNA[24] to the negative chamber of a chip containing a single 4 nm nanopore. Upon the addition of DNA, the ion current developed sharp blockade spikes,[3] which corresponded to the translocation of individual DNA molecules through the pore (Fig. 6a). Figure 6b displays an expanded view of three translocation events. One striking feature of these translocation events is the relatively large current blockade compared with previous reports:[12,13] this may be due to our pore structure. An extensive characterization of the DNA translocation dynamics using these pores will be the subject of a future publication.

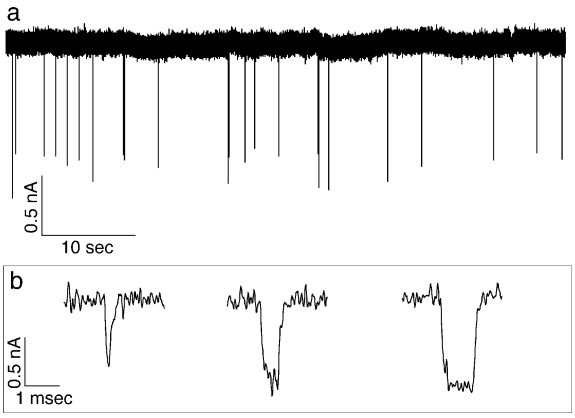

Figure 6. a) Typical current trace of a 4 nm nanopore at 1 M KCl after the addition of 10 nM double-stranded DNA (150 bp; bp = base pair), measured using a bias of 400 mV. Discrete drops in the ion current are clearly observed, corresponding to pore blockades due to translocation of DNA molecules. b) Three translocation events shown on an expanded scale.

In summary, we have developed and optimized a procedure for rapid nanopore and nanopores array fabrication in thin Si_3N_4 membranes. Our procedure yields highly tunable and reproducible nanopores in the range of 2–20 nm. Characterization of our nanopores revealed a truncated double-cone structure, resulting in an effective nanopore thickness of 17 nm, which was about a third of the membrane thickness. As with previous reports, we found that the pore-expansion/contraction dynamics depend on its initial size, as well as on the e-beam intensity. Controlled contraction/expansion allowed the nanopore dimensions to be tuned with sub-nanometer accuracy (0.5 nm). Another important attribute of our procedure is its short fabrication time of ca. 30 s. The achieved accuracy and speed favorably compare with previous reports, allowing the rapid fabrication of nanopore arrays by automated STEM. In addition to highly parallelized DNA and protein analysis afforded by nanopore arrays using a combination of electrical and optical detection, rapid array fabrication may offer a wide range of other applications, such as ultrasensitive nanometer-scale filtration devices.

Received: June 1, 2006
Revised: August 8, 2006

[1] L. Song, M. R. Hobaugh, C. Shustak, S. Cheley, H. Bayley, J. E. Gouaux, *Science* **1996**, *274*, 1859.

[2] a) J. J. Kasianowicz, E. Brandin, D. Branton, D. W. Deamer, *Proc. Natl. Acad. Sci. USA* **1996**, *93*, 13 770. b) M. Akeson, D. Branton, J. J. Kasianowicz, E. Brandin, D. W. Deamer, *Biophys. J.* **1999**, *77*, 3227. c) A. Meller, L. Nivon, E. Brandin, J. Golovchenko, D. Branton, *Proc. Natl. Acad. Sci. USA* **2000**, *97*, 1079. d) A. Meller, D. Branton, *Electrophoresis* **2002**, *23*, 2583. e) S. E. Henrickson, M. Misakian, B. Robertson, J. J. Kasianowicz, *Phys. Rev. Lett.* **2000**, *85*, 3057. f) J. Nakane, M. Akeson, A. Marziali, *Electrophoresis* **2002**, *23*, 2592. g) A. Meller, *J. Phys.: Condens. Matter* **2003**, *15*, R581. h) M. Bates, M. Burns, A. Meller, *Biophys. J.* **2003**, *84*, 2366. i) W. Wang, T. Lee, I. Kretzschmar, M. A. Reed, *Nano Lett.* **2004**, *4*, 643. j) J. Mathe, A. Aksimentiev, D. R. Nelson, K. Schulten, A. Meller, *Proc. Natl. Acad. Sci. USA* **2005**, *102*, 12 377. k) T. Z. Butler, J. H. Gundlach, M. A. Troll, *Biophys. J.* **2006**, *90*, 190.

[3] A. Meller, L. Nivon, D. Branton, *Phys. Rev. Lett.* **2001**, *86*, 3435.

[4] a) A. F. Sauer-Budge, J. A. Nyamwanda, D. K. Lubensky, D. Branton, *Phys. Rev. Lett.* **2003**, *90*, 238 101. b) J. Mathe, H. Visram, V. Viasnoff, Y. Rabin, A. Meller, *Biophys. J.* **2004**, *87*, 3205. c) J. Nakane, M. Wiggin, A. Marziali, *Biophys. J.* **2004**, *87*, 615. d) J. Mathe, A. Arinstein, Y. Rabin, A. Meller, *Europhys. Lett.* **2006**, *73*, 128.

[5] a) W. Vercoutere, S. Winters-Hilt, H. Olsen, D. Deamer, D. Haussler, M. Akeson, *Nat. Biotechnol.* **2001**, *19*, 248. b) S. Howorka, L. Movileanu, O. Braha, H. Bayley, *Proc. Natl. Acad. Sci. USA* **2001**, *98*, 12 996. c) W. A. Vercoutere, S. Winters-Hilt, V. S. DeGuzman, D. Deamer, S. E. Ridino, J. T. Rodgers, H. E. Olsen, A. Marziali, M. Akeson, *Nucleic Acids Res.* **2003**, *31*, 1311.

[6] B. Hornblower, A. Coombs, R. Whitaker, A. Kolomeisky, A. Meller, M. Akeson, unpublished.

[7] a) J. J. Kasianowicz, D. L. Burden, L. C. Han, S. Cheley, H. Bayley, *Biophys. J.* **1999**, *76*, 837. b) L. Q. Gu, O. Braha, S. Conlan, S. Cheley, H. Bayley, *Nature* **1999**, *398*, 686. c) O. Braha, L. Q. Gu, L. Zhou, X. Lu, S. Cheley, H. Bayley, *Nat. Biotechnol.* **2000**, *18*, 1005. d) L. Movileanu, S. Cheley, S. Howorka, O. Braha, H. Bayley, *J. Gen. Physiol.* **2001**, *117*, 239.

[8] J. Li, D. Stein, C. McMullan, D. Branton, M. J. Aziz, J. A. Golovchenko, *Nature* **2001**, *412*, 166.

[9] T. Mitsui, D. Stein, Y. R. Kim, D. Hoogerheide, J. A. Golovchenko, *Phys. Rev. Lett.* **2006**, *96*, 014 307.

[10] A. J. Storm, J. H. Chen, X. S. Ling, H. W. Zandbergen, C. Dekker, *Nat. Mater.* **2003**, *2*, 537.

[11] a) T. A. Desai, D. J. Hansford, L. Leoni, M. Essenpreis, M. Ferrari, *Biosens. Bioelectron.* **2000**, *15*, 453. b) M. Karhanek, J. T. Kemp, N. Pourmand, R. W. Davis, C. D. Webb, *Nano Lett.* **2005**, *5*, 403. c) J. Nilsson, J. R. I. Lee, T. V. Ratto, S. E. Letant, *Adv. Mater.* **2006**, *18*, 427. d) G. L. Wang, B. Zhang, J. R. Wayment, J. M. Harris, H. S. White, *J. Am. Chem. Soc.* **2006**, *128*, 7679. e) C. C. Harrell, Z. S. Siwy, C. R. Martin, *Small* **2006**, *2*, 194.

[12] a) J. Li, M. Gershow, D. Stein, E. Brandin, J. A. Golovchenko, *Nat. Mater.* **2003**, *2*, 611. b) A. J. Storm, J. H. Chen, H. W. Zandbergen, C. Dekker, *Phys. Rev. E: Stat., Nonlinear, Soft Matter Phys.* **2005**, *71*, 051 903. c) A. J. Storm, C. Storm, J. Chen, H. Zandbergen, J. F. Joanny, C. Dekker, *Nano Lett.* **2005**, *5*, 1193.

[13] J. B. Heng, C. Ho, T. Kim, R. Timp, A. Aksimentiev, Y. V. Grinkova, S. Sligar, K. Schulten, G. Timp, *Biophys. J.* **2004**, *87*, 2905.

[14] V. Viasnoff, A. Meller, presented at Bioimage Summer School Paris, Paris, France, July 2005.

[15] D. Krapf, M. Y. Wu, R. M. Smeets, H. W. Zandbergen, C. Dekker, S. G. Lemay, *Nano Lett.* **2006**, *6*, 105.

[16] M. Y. Wu, D. Krapf, M. Zandbergen, H. Zandbergen, P. E. Baton, *Appl. Phys. Lett.* **2005**, *87*, 113 106.

[17] a) A. J. Storm, J. H. Chen, X. S. Ling, H. W. Zandbergen, C. Dekker, *J. Appl. Phys.* **2005**, *98*, 036 102. b) H. Chang, F. Kosari, G. Andreadakis, M. A. Alam, G. Vasmatzis, R. Bashir, *Nano Lett.* **2004**, *4*, 1551.

[18] D. Chescoe, P. J. Goodhew, *The Operation of Transmission and Scanning Electron Microscopes*, Oxford University Press, New York **1990**.

[19] The electron intensity was measured using an in-holder electrometer.

[20] N. Maluf, K. Williams, *An Introduction to Microelectromechanical Systems Engineering*, Artech House Publishers, Boston **2004**.

[21] Sample was imaged at 40 000× magnification using a JEOL JEM2200FS operating at 200 keV, equipped with an Omega-type energy filter set to a slit width of 30 eV. A single-axis tilt series of 46 images were recorded from –45° to +45° with a tilt increment of 2° using a Gatan Ultrascan 4k × 4k charge-coupled device (CCD) camera in conjunction with the SerialEM automated-tilt-series acquisition software. The final pixel size of the image was 1.24 nm after an interpolation of the image size. Image processing of the tilt series were carried out using the IMOD software suite. Individual projection images of the tilt series were aligned with cross correlation and the tomographic reconstruction was calculated by weighted back-projection.

[22] C. J. Lo, T. Aref, A. Bezryadin, *Nanotechnology* **2006**, *17*, 3264.

[23] The calculation was performed by integration of the volume of the nanopore for the resistance, assuming a truncated double-cone structure.

[24] The DNA fragment (150 bp) was purchased from Fermentas, and its purity was verified by gel electrophoresis.